HHS Public Access

Author manuscript

Biochemistry. Author manuscript; available in PMC 2017 July 26.

Published in final edited form as:

Biochemistry. 2016 July 26; 55(29): 4077–4084. doi:10.1021/acs.biochem.6b00546.

Activation Mechanism of the *Bacteroides fragilis* Cysteine Peptidase, Fragipain

Julien Herrou[†], **Vivian M. Choi**[‡], **Juliane Bubeck Wardenburg**[‡,§], and **Sean Crosson**[†,‡,*]

[†]Department of Biochemistry and Molecular Biology, University of Chicago, 929 East 57th Street, Chicago, Illinois 60637, United States

[‡]Department of Microbiology, University of Chicago, 929 East 57th Street, Chicago, Illinois 60637, United States

[§]Department of Pediatrics, University of Chicago, 929 East 57th Street, Chicago, Illinois 60637, United States

Abstract

Enterotoxigenic *Bacteroides fragilis* produces a secreted metalloprotease known as *B. fragilis* toxin (BFT), which contributes to anaerobic sepsis, colitis, and colonic malignancy in mouse models of disease. A C11 family cysteine protease, fragipain (Fpn), directly activates BFT in the *B. fragilis* cell by removing the BFT prodomain. Fpn is itself a proenzyme and is autoactivated upon cleavage at an arginine residue in its activation loop. We have defined the proteolytic active site of Fpn, demonstrated that Fpn autoactivation can occur by an *in trans* loop cleavage mechanism, and characterized structural features of the Fpn activation loop that control peptidase activity against several substrates, including BFT. An arginine residue at the autocleavage site determines the fast activation kinetics of Fpn relative to the homologous C11 protease, PmC11, which is cleaved at lysine. Arginine to alanine substitution at the cleavage site ablated peptidase activity, as did partial truncation of the Fpn activation loop. However, complete truncation of the activation loop yielded an uncleaved, pro form of Fpn that was active as a peptidase against both Fpn and BFT substrates. Thus, Fpn can be transformed into an active peptidase in the absence of activation loop cleavage. This study provides insight into the mechanism of fragipain activation and, more generally, defines the role of the C11 activation loop in the control of peptidase activity and substrate specificity.

Graphical abstract

[*]**Corresponding Author**. scrosson@uchicago.edu.

ASSOCIATED CONTENT

Supporting Information

The Supporting Information is available free of charge on the ACS Publications website at DOI: 10.1021/acs.biochem.6b00546.

Three figures and two tables (PDF)

The authors declare no competing financial interest.

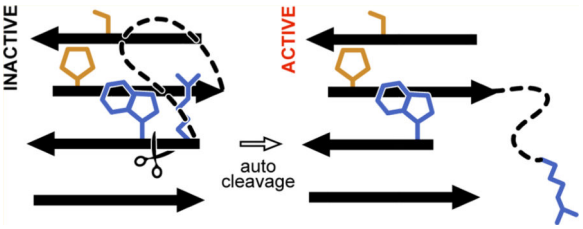

Bacteroides spp. are the predominant anaerobes in the human gut, where they maintain a generally beneficial relationship with the host.[1–3] However, these bacteria can escape the gastrointestinal tract and cause disease.[1,3–8] *Bacteroides fragilis* is the leading cause of anaerobic sepsis and bacteremia in humans[4–6,9] and possesses virulence factors that allow survival outside the host digestive tract and determine pathogenicity.[1] Among the primary *B. fragilis* virulence determinants is a metalloprotease toxin known as fragilysin, or BFT, which is expressed by enterotoxigenic strains.[10–14] BFT contributes to sepsis and pro-inflammatory disease within the colon by cleaving cadherin family proteins and thereby compromising tissue barrier integrity.[15–18] BFT is synthesized as an inactive zymogen that consists of an N-terminal prodomain, a flexible linker, and a C-terminal catalytic domain.[13] It is activated through cleavage of an arginine-containing site in its flexible linker[11,13] by a peptidase known as fragipain (Fpn),[18] a member of the C11 clostripain family.[19–22]

An X-ray crystal structure of Fpn revealed a cysteine-histidine catalytic dyad with cleavage specificity for Arg–Xaa bonds.[18] Notably, Fpn contains its own arginine-containing cleavage site (R147/W148) within a flexible loop and, like clostripains[23–25] and related proteases,[22,26–29] is self-cleaving. The crystal structure of Fpn captured the protein in a *trans*-cleaved state with the loop arginine projecting into the active site of an adjacent Fpn molecule in the crystal lattice.[18] As observed in related cysteine proteases,[29–33] autocleavage is presumed to enhance Fpn peptidase activity by changing active site accessibility and/or restructuring catalytic residues. The goal of this study was to assess the *trans* autocleavage mechanism suggested by the Fpn crystal structure and to characterize the role of the cleavage loop in control of Fpn peptidase activity.

We expressed and purified a set of Fpn loop and active site mutants and evaluated their autopeptidase activities and their ability to process BFT. We demonstrate that an intact Cys-His active site is required for autocleavage and BFT cleavage, and that Fpn can cut itself *in trans*. Substitution of arginine with lysine at the Fpn cleavage site reduced autopeptidase activity, while arginine to alanine substitution ablated Fpn autocleavage and BFT processing. Truncating the Fpn cleavage loop by five residues resulted in a total loss of peptidase activity, while complete removal of this same loop yielded an enzyme that was uncleaved yet active as a peptidase against Fpn and BFT substrates. Thus, loop removal results in a pro form of Fpn that is enzymatically active, albeit less active than wild-type Fpn. Our data provide evidence of a model in which the Fpn cleavage loop functions to regulate peptidase activity both by steric occlusion of the Fpn active site and by controlling the active site conformation.

MATERIALS AND METHODS

Recombinant Expression Plasmids

Strains expressing wild-type Fpn, $Fpn^{H135A+C180A}$, and BFT have been described previously.[18] Primers used to introduce deletions and produce Fpn^{R147K}, Fpn^{R147A}, $Fpn^{L\Delta5}$, $Fpn^{L\Delta7}$, and $Fpn^{L\Delta7+R147A}$ mutant proteins are listed in Table S1. pET-upstream and T7-term primers were used to amplify the different inserts, and the pET28-*fpn* plasmid was used as a template. The 19 N-terminal amino acids of Fpn, corresponding to the lipoprotein signal sequence, were absent from the tagged recombinant proteins. After purification, the different polymerase chain reaction products were digested with NcoI–NotI restriction enzymes and ligated into the pET28c expression plasmid (Kan^R). Plasmids were then transformed into *Escherichia coli* Top10. After sequencing, plasmids with the different inserts were purified and transformed into the *E. coli* Rosetta (DE3) pLysS strain for protein expression (see Table S2 for strain information).

Protein Expression and Purification

A 50 mL overnight Luria broth (LB, Fisher Scientific) culture inoculated with the protein expression strains (see Table S2 for strain information) was used to inoculate 300 mL of LB medium supplemented with the appropriate antibiotics. Overexpression of C-terminally His-tagged Fpn and BFT proteins was induced at an OD_{600} of ~0.8 (37 °C, 220 rpm) by adding 1 mM isopropyl β-D-1-thiogalactopyranoside (IPTG, GoldBio). After being induced for 5 h, cells were harvested by centrifugation at 11000*g* for 20 min at 4 °C. Cell pellets were resuspended in 10 mL of 10 mM Tris-HCl (pH 7.4), 150 mM NaCl, and 10 mM imidazole buffer supplemented with 5 μg/mL DNase I. Cells were disrupted by one passage in a microfluidizer (Microfluidics LV1). The resulting cell lysate was clarified by centrifugation at 39000*g* for 20 min at 4 °C.

Purification of His-tagged proteins was performed using nickel affinity chromatography (NTA resin, GE Healthcare). After the clarified lysate samples had been bound to the column, three washing steps were performed using 10, 75, and 200 mM imidazole Tris-NaCl buffers followed by elution with 500 mM imidazole Tris-NaCl buffer. All purification steps were performed at 4 °C. The protein purity of the different samples was assessed with a 14% sodium dodecyl sulfate–polyacrylamide gel electrophoresis (SDS–PAGE) gel stained with Coomassie Blue. For every construct, protein concentrations were estimated by UV absorption spectroscopy (280 nm) using a NanoDrop 1000 spectrophotometer (Thermo Scientific).

Protease Cleavage Assays

After purification, the different Fpn mutant proteins as well as BFT were dialyzed overnight against a Tris-NaCl buffer containing 10 mM Tris (pH 7.4) and 150 mM NaCl. To assess peptidase digestion patterns, 5 μL of the different Fpn mutant proteins (at 20 μM) was mixed with 5 μL of wild-type Fpn or $Fpn^{H135A+C180A}$ proteins (at 20 μM) or with 5 μL of the BFT toxin (at 20 μM). These 10 μL reaction mixtures were then incubated at 37 °C for 45 min. After incubation, 5 μL of SDS–PAGE loading buffer was added to the reaction mixture and

boiled for 2 min at 95 °C. These 15 μL samples were then completely loaded on a 14% SDS–PAGE gel, resolved, and Coomassie stained.

N_α-Benzoyl-L-arginine Ethyl Ester (BAEE) Assay

One milliliter of phosphate buffer [67 mM NaH_2PO_4 (pH 7.5)] containing 200 nM wild-type or mutant Fpn proteins was mixed with 1.25 mM BAEE. The absorbance at 253 nm was measured using a UV–vis spectrophotometer (Shimadzu UV-1650pc) and a quartz cuvette. Experiments were conducted in triplicate.

Protease Kinetic Assay

After purification and dialysis, 100 μL of a solution containing 5 μM wild-type Fpn or $Fpn^{L\Delta7+R147A}$ and 5 μM BFT or $Fpn^{H135+C180A}$ was incubated at 37 °C. Aliquots (10 μL) were taken at regular time intervals, mixed with 5 μL of SDS–PAGE loading buffer, and boiled for 2 min at 95 °C. The 15 μL samples were then loaded and resolved on a 14% SDS–PAGE gel and Coomassie stained. After destaining, intensities of the bands corresponding to cleaved BFT or $Fpn^{H135+C180A}$ were quantified using ImageJ[34] and converted into a percent cleaved value. Data were plotted and fitted using Prism. Digestion kinetic assays were conducted in triplicate with three independent purifications of each protein.

Generation of *B. fragilis* Strains

To introduce *fpn* mutant alleles into a Δ*fpn B. fragilis* strain, the replicating pAH2 plasmid (Cli^R) was used (gift of A. Hecht); cloning details were previously described.[18]

Western Blot Analysis

Preparation of *B. fragilis* cell lysates and supernatants for Western blot analysis was performed as previously described,[18] using the following primary and secondary antibodies: α-Fpn rabbit polyclonal antisera (1:2500), α-BFT rabbit polyclonal antisera (1:2000), α-RpoA (1:20000), and α-rabbit Alexa Fluor 680.

Protein Structure Alignments

Structural alignments and root-mean-square deviation (rmsd) calculations were performed using PyMOL (PyMOL Molecular Graphics System, version 1.7.4, Schrödinger, LLC). Residue substitutions in the Fpn active site were performed using Coot.[35]

RESULTS

The Cysteine Protease Fpn Can Autocleave *in Trans*

In a previous study,[18] we crystallized and determined the structure of the Fpn cysteine protease [Protein Data Bank (PDB) entry 5DYN (http://dx.doi.org/10.15785/SBGRID/225)]. This structure uniquely captured the active site bound to the cleaved loop of an adjacent Fpn molecule *in trans* (Figure 1A). The site of Fpn autocleavage is contained in a flexible loop region of eight residues that connect β-strand 6 to β-strand 7. Within β-strand 6 is a histidine residue (H135) that forms the protein active site with a proximal cysteine (C180) (Figure 1A,B). The structure of Fpn is similar to that of the clostripain-like protein PmC11 of

Parabacteroides merdae,[36] which has an identical fold, and a closely related active site and loop cleavage site (Figure 1C). Though PmC11 and Fpn have a low level of structural homology to cysteine proteases such as legumain (PDB entry 4AW9),[30] caspase-3 (PDB entry 1NMS),[37] and gingipain (PDB entry 4RBM),[38] the active sites are related (Figure 1C). However, cleavable activation loops are not present at equivalent positions in these proteases. This suggests that the activation loop present in the C11 peptidases Fpn and PmC11 may serve a unique structural role in controlling peptidase activity.

The Fpn crystal structure provided evidence of a model in which the loop is cut *in trans*. To test this model, we first generated and purified Fpn active site mutant protein ($Fpn^{H135A+C180A}$). Purified $Fpn^{H135A+C180A}$ resolved as a single polypeptide by SDS–PAGE, confirming that this mutant has no autocleavage activity (Figure 1D). Wild-type Fpn resolved as two bands (at ≈14 and 28 kDa), consistent with autocleavage at a single site. It was not known whether wild-type Fpn autocleaves *in cis, in trans*, or both. As such, we tested whether wild-type Fpn could cut $Fpn^{H135A+C180A}$ *in trans*. We mixed the two proteins, incubated them for 45 min at 37 °C, and resolved the mixture by SDS–PAGE. The high-molecular weight band at ≈42 kDa corresponding to uncleaved and inactive $Fpn^{H135A+C180A}$ disappeared, and we observed only the two cut bands on a gel (Figure 1D). This provides evidence that $Fpn^{H135A+C180A}$ is cut by wild-type Fpn *in trans* and supports the *trans*-cleavage activation mechanism evidenced by our crystal structure. We further tested the concentration dependence of this cleavage reaction by mixing 5 μL of inactive $Fpn^{H135A+C180A}$ (20 μM) with 5 μL of wild-type Fpn at various concentrations (from 20 to 0.01 μM). After being incubated at 37 °C for 5 min, samples were resolved by SDS–PAGE. Cleavage of $Fpn^{H135A+C180A}$ by wild-type Fpn is concentration-dependent; 0.125 μM wild-type Fpn was not sufficient to completely cleave $Fpn^{H135A+C180A}$ (Figure S1).

We next tested whether Fpn activity required divalent cations as described for some cysteine proteases.[22] We performed the same cleavage experiment between wild-type Fpn and the $Fpn^{H135A+C180A}$ active site mutant in the presence of 50 mM EDTA. After incubation for 45 min at 37 °C, the band corresponding to uncleaved $Fpn^{H135A+C180A}$ was absent, providing evidence that Fpn peptidase activity does not require divalent cations (Figure 1D). This confirms what has been described for *Parabacteroides merdae* PmC11.[36]

Fpn and PmC11 Have Related Structures and Active Sites but Differing Autocleavage Kinetics

P. merdae PmC11 (PDB entry 3UWS)[36] and *B. fragilis* Fpn (PDB entry 5DYN)[18] have 35% identical sequences and a high degree of overall tertiary structural homology (rmsd of Cα coordinates = 0.81 Å) (Figure 2A). Differences in structure are evident in the cleavable loop. An additional loop (Q238–G254) is present in only Fpn and acts like a lid, partially covering the active site. In the Fpn crystal structure, the cleavable loop is eight residues long, cut, and unfolded and terminates at an arginine residue (R147). The corresponding loop in PmC11 is longer (10 amino acids) and helical and terminates at a lysine residue (K147) (Figures 1C and 2A,B). We tested whether substitution of R147 with lysine (as observed in PmC11) affects autocleavage. Like PmC11,[36] Fpn^{R147K} was purified as a partially cleaved protein that resolved as three bands as determined by SDS–PAGE (at ≈42, 28, and 14 kDa) (Figure

2C). A 16 h incubation at 37 °C resulted in complete cleavage of the protein, providing evidence that a lysine-containing cleavage site is not as efficient a substrate as an arginine-containing site for this class of peptidase. When we compared the ability of wild-type Fpn and fully processed Fpn^{R147K} mutant protein to cleave the synthetic substrate N_{α}-benzoyl-L-arginine ethyl ester (BAEE), both proteins showed equivalent activities. Thus, Fpn^{R147K} has specifically reduced cleavage kinetics for the lysine-containing polypeptide in the cleavage loop but not for the small substrate BAEE (Figure 2D).

We then compared the structures of the Fpn and PmC11 active sites. Six residues differ between Fpn and PmC11. Only residues D52, D178, and G207 interact with the R147 side chain in Fpn (Figure 2E,F). In PmC11 cocrystallized with a peptide-like inhibitor (PDB entry 4YEC), the side chain of the terminal lysine residue interacts with D177 only (Figure 2E). Given these structural data, substitution of R147 with lysine is predicted to result in fewer polar contacts with the surrounding residues present in the Fpn active site (Figure 2G). This may explain the difference in autocleavage kinetics between Fpn and PmC11.

Loop Cleavage Activates Fpn Peptidase

We tested whether an Fpn mutant with an intact active site but missing the arginine at the cleavage site (Fpn^{R147A}) would cut *in trans*. A cleaved protein runs as two fragments (≈14 and 28 kDa) on a SDS–PAGE gel (Figure 3A,B). Like $Fpn^{H135A+C180A}$, an Fpn^{R147A} mutant was purified as a single polypeptide with a molecular weight of ≈42 kDa, demonstrating that it was uncleaved (Figure 3C). Mixing Fpn^{R147A} with $Fpn^{H135A+C180A}$ yielded no cleaved product. This provides evidence that Fpn loop cleavage is a required step in activation of Fpn peptidase function. As a positive control, we assessed $Fpn^{H135A+C180A}$ cleavage by wild-type Fpn at the same time interval and observed *trans* cutting (Figure 3B). Wild-type Fpn failed to cleave Fpn^{R147A}, demonstrating that mutation of the arginine at the cleavage site ablates cutting by wild-type Fpn *in trans* (Figure 3C).

Partial Truncation of the Cleavage Loop Results in Lower *in Trans* Peptidase Activity

As described above, the Fpn cleavage site (R147/W148) is positioned at the end of a eight-residue flexible loop (…WIPSPAKT**R**/**W**…). We hypothesized that this loop physically occludes the accessibility of the active site to the substrate. Loop cleavage may serve to increase active site accessibility and permit *in trans* peptidase activity. To test this hypothesis, we engineered a small loop (L) mutant from which five amino acids (ΔS142–T146) were deleted. Purified $Fpn^{L\Delta5}$ resolved as a single 42 kDa band by SDS–PAGE (Figure 3D). This protein was incapable of cleaving the $Fpn^{H135A+C180A}$ active site mutant *in trans* and could not be cleaved by wild-type Fpn *in trans* (Figure 3D). Thus, removing these five residues of the Fpn cleavage loop either blocks accessibility of the active site or introduces structural constraints on Fpn that are incompatible with peptidase activity.

Complete Removal of the Fpn Cleavage Loop Yields an Enzyme That Is Active in the Pro Form

To further explore the functional role of the Fpn cleavage loop, we engineered an additional Fpn mutant with the entire loop region deleted (ΔI140–T146). On the basis of published cysteine protease structures, complete loop deletion should result in an active site that is

closer in geometry to the legumain, gingipain, or caspase-3 active sites (Figure 1C). This "loopless" mutant ($Fpn^{L\Delta7}$) resolved as an uncleaved 42 kDa polypeptide by SDS–PAGE. Though $Fpn^{L\Delta7}$ was evidently in the pro form, it was capable of cleaving $Fpn^{H135A+C180A}$ *in trans*. Wild-type Fpn did not cleave loopless Fpn *in trans* (Figure 3E). To rule out the possibility that the observed peptidase activity of $Fpn^{L\Delta7}$ was due to a small amount of cleaved protein present in the sample, we engineered a mutant with an alanine at the cleavage site. This mutant ($Fpn^{L\Delta7+R147A}$) had the same characteristics as $Fpn^{L\Delta7}$: it was purified as a single polypeptide, cleaved $Fpn^{H135A+C180A}$, and could not be processed by wild-type Fpn (Figure 3F). We conclude that complete removal of the cleavable loop of Fpn results in a pro form of the enzyme that is enzymatically active; i.e., $Fpn^{L\Delta7}$ does not require loop cleavage for activity. A table summarizing the activity and cleavability of each Fpn mutant is presented in Figure 3G.

Loopless Fpn Processes the Metalloprotease Toxin BFT

In *B. fragilis*, a target of Fpn is the metalloprotease toxin BFT.[18] Cleavage of pro-BFT by Fpn activates BFT, which proteolyzes E-cadherin and VE-cadherin in the mammalian host. We tested the ability of our different Fpn mutants to cleave pro-BFT. The primary Fpn cut site in BFT is located after residue R211; an alternative but minor cut site is present after residue R162.[18] As expected, BFT was cut by wild-type Fpn, which resulted in a 17 kDa BFT fragment on a SDS–PAGE gel. The active site mutant protein ($Fpn^{H135A+C180A}$), the cleavage site mutant protein (Fpn^{R147A}), or the "short" deletion loop mutant protein ($Fpn^{L\Delta5}$) had no observable enzymatic activity against BFT after incubation for 45 min at 37 °C (Figure 4). However, the loopless mutant proteins ($Fpn^{L\Delta7}$ and $Fpn^{L\Delta7+R147A}$) cleaved BFT. This demonstrates that the loopless pro form mutants of Fpn can process BFT as a substrate (Figure 4).

Loopless Pro-Fpn Has a Peptidase Activity Lower Than That of Wild-Type Fpn

We next measured activities of the different Fpn mutants using BAEE as a substrate. As expected, wild-type Fpn had high activity while $Fpn^{H135A+C180A}$ and Fpn^{R147A} were inactive (Figure 5A). Surprisingly, the loopless mutant, $Fpn^{L\Delta7+R147A}$, was also unable to process BAEE (Figure 5A). This is inconsistent with our result showing that $Fpn^{L\Delta7+R147A}$ cleaves $Fpn^{H135A+C180A}$ and BFT as substrates. We hypothesize that complete loop removal may have introduced some structural constraints in or near the active site that reduce activity against the smaller substrate, BAEE.

The absence of detectable enzymatic activity of $Fpn^{L\Delta7+R147A}$ against BAEE suggested that the $Fpn^{L\Delta7+R147A}$ cleavage rate of $Fpn^{H135A+C180A}$ and BFT may be slow in comparison to that of the wild type. To test this hypothesis, we evaluated the $Fpn^{L\Delta7+R147A}$ cleavage rate using $Fpn^{H135A+C180A}$ or BFT as the substrate. Briefly, loopless $Fpn^{L\Delta7+R147A}$ was mixed with $Fpn^{H135A+C180A}$ or BFT and incubated at 37 °C. Samples were taken at different time points and visualized by SDS–PAGE. Intensities of cleaved $Fpn^{H135A+C180A}$ and BFT bands were quantified and plotted (representative SDS–PAGE gels are shown in Figure S2). Compared to that of the wild type, loopless $Fpn^{L\Delta7+R147A}$ had a lower apparent activity. $Fpn^{L\Delta7+R147A}$ took approximately 45 min to process $Fpn^{H135A+C180A}$ (Figure 5B) or BFT (Figure 5C). In comparison, wild-type Fpn processed $Fpn^{H135A+C180A}$ (Figure 5B) or BFT

(Figure 5C) in approximately 5 min. Thus, loopless Fpn$^{L\Delta7+R147A}$ is less efficient at processing Fpn and BFT substrates.

To assess whether the activities of Fpn mutants measured *in vitro* reflect the activity in *B. fragilis* cells, we measured *B. fragilis* BFT levels by Western blotting in *fpn* mutant backgrounds. Consistent with our *in vitro* results, a *B. fragilis* strain expressing only uncleaved, loopless *fpn* (Δ*fpn*/pAH2-*fpn*$^{L\Delta7}$) processed BFT, but with an efficiency lower than that of a *B. fragilis* Δ*fpn*/pAH2-*fpn* strain. Control strains *B. fragilis* Δ*fpn* and Δ*fpn*/pAH2-*fpn*$^{H135A+C180A}$ did not show any cleaved BFT by Western blotting (Figure S3).

DISCUSSION

Cysteine proteases are regulated in multiple ways, including interaction with protein inhibitors, or by inhibitory domains *in cis*.[33,39,40] The *B. fragilis* cysteine protease Fpn contains an inhibitory loop domain that is autocleaved, which results in enzyme activation. We previously reported a crystal structure of a cleaved form of Fpn in which this loop occupies a conformation that is compatible with an *in trans* autocleavage mechanism.[18] In this structure, Fpn is cut at an arginine residue that is positioned between the histidine and cysteine of the catalytic dyad of an adjacent molecule in the crystal lattice and forms a covalent bond with the cysteine side chain (Figure 1A). To the best of our knowledge, an equivalent configuration in a cysteine protease has only been observed in a structure of cathepsin L, in which the cleaved region was trapped in the active site of a neighboring molecule.[41] Biochemical data presented in this study support a *trans* model of Fpn cleavage but do not rule out the possibility that Fpn can also autocleave *in cis*.

The closest homologue of Fpn in the PDB is *P. merdae* PmC11.[36] Fpn and PmC11 are 35% identical at the primary structure level and exhibit a high degree of tertiary structural similarity (rmsd of Cα coordinates of <1 Å). A comparison of the active sites and the cleavage sites of these structures reveals some differences (Figure 2A,B,E) that we propose have important consequences in Fpn and PmC11 autocleavage kinetics. Briefly, Fpn expressed in a heterologous *E. coli* system is purified as a fully cleaved active enzyme that resolves as two bands by SDS–PAGE (Figures 1D and 3B), while PmC11 is purified as a population of cleaved and uncleaved (i.e., active and inactive, respectively) protein that is processed to completion after 16 h at 37 °C.[36] The difference in autocleavage kinetics between these related proteins can be attributed to the lysine residue (K147) in the PmC11 cleavable loop (Figure 2B). Weakened molecular interaction of K147 relative to that of R147 (Figure 2F,G) is predicted to reduce stability of the active site–loop interaction and slow the cleavage reaction. This is supported by our data showing that replacement of R147 with lysine reduces the rate of Fpn autocleavage (Figure 2C) and by the published observation that PmC11 has a stronger preference for substrates containing arginine over those containing lysine.[36] Slower autoprocessing kinetics may have some physiological importance in *P. merdae*, though the *in vivo* substrate of PmC11 remains undefined. *P. merdae* does not encode a homologue of BFT.

The extended loop conformation captured in the Fpn crystal structure (Figure 1A) suggests a minimum loop length requirement for Fpn to be cut *in trans*. We have shown that a loop

truncated by five residues cannot be cut *in cis* or *in trans*, even if the proper residue identity of cleavage site is intact (Figure 3D). However, complete removal of the loop results in an active site that more closely resembles caspases, legumain, or gingipain (Figure 1C). This loopless Fpn mutant has clear peptidase activity even though the enzyme remains in an uncleaved pro form (Figures 3E,F and 4). Together, these results suggest that the cleavage loop may function both to limit access to the active site and to control the conformation of active site residues required for peptide bond cleavage. Structures of uncleaved Fpn mutants will provide deeper insight into the molecular basis of loop inhibition.

In conclusion, we provide new structural insight into how the cleavable loop of C11 family peptidases controls activity. We demonstrate that Fpn can be activated by loop cleavage *in trans*. We successfully engineered an active pro form of Fpn, though this loopless mutant ($Fpn^{L\Delta7+R147A}$) processed substrates more slowly than wild-type Fpn did (Figure 5A–C). We postulate that β-strands 6 and 7, which contain the catalytic dyad, are more flexible in the cleaved wild-type form of Fpn and can thus accommodate and process a wider range of substrates more efficiently than the constrained, loopless Fpn can. Nevertheless, the fact that we are able to produce an active version of pro-Fpn by loop removal suggests that modifications of the loop region may be a general approach to engineering C11 family cysteine proteases with variable substrate specificities and peptidase activities.

Supplementary Material

Refer to Web version on PubMed Central for supplementary material.

Acknowledgments

Funding

This work was supported in part by a Pilot and Feasibility Award from the Digestive Diseases Research Core Center at the University of Chicago (National Institute of Diabetes and Digestive and Kidney Diseases Grant P30DK42086). V.M.C. received support from the National Institutes of Health Medical Scientist Training Program at the University of Chicago (GM007281).

The authors thank members of the Crosson lab for useful discussion.

REFERENCES

1. Wexler HM. Bacteroides: the good, the bad, and the nitty-gritty. Clin Microbiol Rev. 2007; 20:593–621. [PubMed: 17934076]
2. Karlsson FH, Ussery DW, Nielsen J, Nookaew I. A closer look at bacteroides: phylogenetic relationship and genomic implications of a life in the human gut. Microb. Ecol. 2011; 61:473–485. [PubMed: 21222211]
3. Wick EC, Sears CL. Bacteroides spp. and diarrhea. Curr. Opin. Infect. Dis. 2010; 23:470–474. [PubMed: 20697287]
4. Redondo MC, Arbo MD, Grindlinger J, Snydman DR. Attributable mortality of bacteremia associated with the Bacteroides fragilis group. Clin. Infect. Dis. 1995; 20:1492–1496. [PubMed: 7548498]
5. Ngo JT, Parkins MD, Gregson DB, Pitout JD, Ross T, Church DL, Laupland KB. Population-based assessment of the incidence, risk factors, and outcomes of anaerobic bloodstream infections. Infection. 2013; 41:41–48. [PubMed: 23292663]

6. Snydman DR, Jacobus NV, McDermott LA, Golan Y, Hecht DW, Goldstein EJ, Harrell L, Jenkins S, Newton D, Pierson C, Rihs JD, Yu VL, Venezia R, Finegold SM, Rosenblatt JE, Gorbach SL. Lessons learned from the anaerobe survey: historical perspective and review of the most recent data (2005–2007). Clin. Infect. Dis. 2010; 50(Suppl. 1):S26–S33. [PubMed: 20067390]
7. Rodrigues C, Siciliano RF, Zeigler R, Strabelli TM. Bacteroides fragilis endocarditis: a case report and review of literature. Braz. J. Infect. Dis. 2012; 16:100–104. [PubMed: 22358367]
8. McHenry MC, Wellman WE, Martin WJ. Bacteremia due to Bacteroides. Review of 11 cases. Arch. Intern. Med. 1961; 107:572–577. [PubMed: 13773998]
9. Robert R, Deraignac A, Le Moal G, Ragot S, Grollier G. Prognostic factors and impact of antibiotherapy in 117 cases of anaerobic bacteraemia. Eur. J. Clin. Microbiol. Infect. Dis. 2008; 27:671–678. [PubMed: 18357478]
10. Moncrief JS, Obiso R Jr, Barroso LA, Kling JJ, Wright RL, Van Tassell RL, Lyerly DM, Wilkins TD. The enterotoxin of Bacteroides fragilis is a metalloprotease. Infect. Immun. 1995; 63:175–181. [PubMed: 7806355]
11. Shiryaev SA, Aleshin AE, Muranaka N, Kukreja M, Routenberg DA, Remacle AG, Liddington RC, Cieplak P, Kozlov IA, Strongin AY. Structural and functional diversity of metalloproteinases encoded by the Bacteroides fragilis pathogenicity island. FEBS J. 2014; 281:2487–2502. [PubMed: 24698179]
12. Franco AA, Mundy LM, Trucksis M, Wu S, Kaper JB, Sears CL. Cloning and characterization of the Bacteroides fragilis metalloprotease toxin gene. Infect. Immun. 1997; 65:1007–1013. [PubMed: 9038310]
13. Goulas T, Arolas JL, Gomis-Ruth FX. Structure, function and latency regulation of a bacterial enterotoxin potentially derived from a mammalian adamalysin/ADAM xenolog. Proc. Natl. Acad. Sci. U. S. A. 2011; 108:1856–1861. [PubMed: 21233422]
14. Van Tassell RL, Lyerly DM, Wilkins TD. Purification and characterization of an enterotoxin from Bacteroides fragilis. Infect. Immun. 1992; 60:1343–1350. [PubMed: 1548060]
15. Wu S, Lim KC, Huang J, Saidi RF, Sears CL. Bacteroides fragilis enterotoxin cleaves the zonula adherens protein, E-cadherin. Proc. Natl. Acad. Sci. U. S. A. 1998; 95:14979–14984. [PubMed: 9844001]
16. Wu S, Shin J, Zhang G, Cohen M, Franco A, Sears CL. The Bacteroides fragilis toxin binds to a specific intestinal epithelial cell receptor. Infect. Immun. 2006; 74:5382–5390. [PubMed: 16926433]
17. Sears CL. The toxins of Bacteroides fragilis. Toxicon. 2001; 39:1737–1746. [PubMed: 11595636]
18. Choi VM, Herrou J, Hecht AL, Teoh WP, Turner JR, Crosson S, Bubeck Wardenburg J. Activation of Bacteroides fragilis toxin by a novel bacterial protease contributes to anaerobic sepsis in mice. Nat. Med. 2016; 22:563–567. [PubMed: 27089515]
19. Rawlings ND, Barrett AJ, Bateman A. MEROPS: the database of proteolytic enzymes, their substrates and inhibitors. Nucleic Acids Res. 2012; 40:D343–D350. [PubMed: 22086950]
20. Kocholaty W, Weil L, Smith L. Proteinase secretion and growth of Clostridium histolyticum. Biochem. J. 1938; 32:1685–1690. [PubMed: 16746798]
21. Kembhavi AA, Buttle DJ, Rauber P, Barrett AJ. Clostripain: characterization of the active site. FEBS Lett. 1991; 283:277–280. [PubMed: 2044766]
22. McLuskey K, Mottram JC. Comparative structural analysis of the caspase family with other clan CD cysteine peptidases. Biochem. J. 2015; 466:219–232. [PubMed: 25697094]
23. Dargatz H, Diefenthal T, Witte V, Reipen G, von Wettstein D. The heterodimeric protease clostripain from Clostridium histolyticum is encoded by a single gene. Mol. Gen. Genet. 1993; 240:140–145. [PubMed: 8341259]
24. Labrou NE, Rigden DJ. The structure-function relationship in the clostripain family of peptidases. Eur. J. Biochem. 2004; 271:983–992. [PubMed: 15009210]
25. Witte V, Wolf N, Diefenthal T, Reipen G, Dargatz H. Heterologous expression of the clostripain gene from Clostridium histolyticum in Escherichia coli and Bacillus subtilis: maturation of the clostripain precursor is coupled with self-activation. Microbiology. 1994; 140(Part 5):1175–1182. [PubMed: 8025682]

26. Klaiman G, Champagne N, LeBlanc AC. Self-activation of Caspase-6 in vitro and in vivo: Caspase-6 activation does not induce cell death in HEK293T cells. Biochim. Biophys. Acta, Mol. Cell Res. 2009; 1793:592–601.
27. Dall E, Brandstetter H. Activation of legumain involves proteolytic and conformational events, resulting in a context-and substrate-dependent activity profile. Acta Crystallogr., Sect. F. Struct. Biol. Cryst. Commun. 2012; 68:24–31.
28. Chen JM, Fortunato M, Barrett AJ. Activation of human prolegumain by cleavage at a C-terminal asparagine residue. Biochem. J. 2000; 352(Part2):327–334. [PubMed: 11085925]
29. Mallorqui-Fernandez N, Manandhar SP, Mallorqui-Fernandez G, Uson I, Wawrzonek K, Kantyka T, Sola M, Thogersen IB, Enghild JJ, Potempa J, Gomis-Ruth FX. A new autocatalytic activation mechanism for cysteine proteases revealed by Prevotella intermedia interpain A. J. Biol. Chem. 2008; 283:2871–2882. [PubMed: 17993455]
30. Dall E, Brandstetter H. Mechanistic and structural studies on legumain explain its zymogenicity, distinct activation pathways, and regulation. Proc. Natl. Acad. Sci. U. S. A. 2013; 110:10940–10945. [PubMed: 23776206]
31. Khan AR, Khazanovich-Bernstein N, Bergmann EM, James MN. Structural aspects of activation pathways of aspartic protease zymogens and viral 3C protease precursors. Proc. Natl. Acad. Sci. U. S. A. 1999; 96:10968–10975. [PubMed: 10500110]
32. Li J, Yuan J. Caspases in apoptosis and beyond. Oncogene. 2008; 27:6194–6206. [PubMed: 18931687]
33. Rzychon M, Chmiel D, Stec-Niemczyk J. Modes of inhibition of cysteine proteases. Acta Biochim. Pol. 2004; 51:861–873. [PubMed: 15625558]
34. Schneider CA, Rasband WS, Eliceiri KW. NIH Image to ImageJ: 25 years of image analysis. Nat. Methods. 2012; 9:671–675. [PubMed: 22930834]
35. Emsley P, Lohkamp B, Scott WG, Cowtan K. Features and development of Coot. Acta Crystallogr., Sect. D. Biol. Crystallogr. 2010; 66:486–501. [PubMed: 20383002]
36. McLuskey K, Grewal JS, Das D, Godzik A, Lesley SA, Deacon AM, Coombs GH, Elsliger MA, Wilson IA, Mottram JC. Crystal Structure and Activity Studies of the C11 Cysteine Peptidase from Parabacteroides merdae in the Human Gut Microbiome. J. Biol. Chem. 2016; 291:9482–9491. [PubMed: 26940874]
37. Erlanson DA, Lam JW, Wiesmann C, Luong TN, Simmons RL, DeLano WL, Choong IC, Burdett MT, Flanagan WM, Lee D, Gordon EM, O'Brien T. In situ assembly of enzyme inhibitors using extended tethering. Nat. Biotechnol. 2003; 21:308–314. [PubMed: 12563278]
38. de Diego I, Veillard F, Sztukowska MN, Guevara T, Potempa B, Pomowski A, Huntington JA, Potempa J, Gomis-Ruth FX. Structure and mechanism of cysteine peptidase gingipain K (Kgp), a major virulence factor of Porphyromonas gingivalis in periodontitis. J. Biol. Chem. 2014; 289:32291–32302. [PubMed: 25266723]
39. Grzonka Z, Jankowska E, Kasprzykowski F, Kasprzykowska R, Lankiewicz L, Wiczk W, Wieczerzak E, Ciarkowski J, Drabik P, Janowski R, Kozak M, Jaskolski M, Grubb A. Structural studies of cysteine proteases and their inhibitors. Acta Biochim. Pol. 2001; 48:1–20. [PubMed: 11440158]
40. Otlewski J, Jelen F, Zakrzewska M, Oleksy A. The many faces of protease-protein inhibitor interaction. EMBO J. 2005; 24:1303–1310. [PubMed: 15775973]
41. Sosnowski P, Turk D. Caught in the act: the crystal structure of cleaved cathepsin L bound to the active site of Cathepsin L. FEBS Lett. 2016; 590:1253–1261. [PubMed: 26992470]

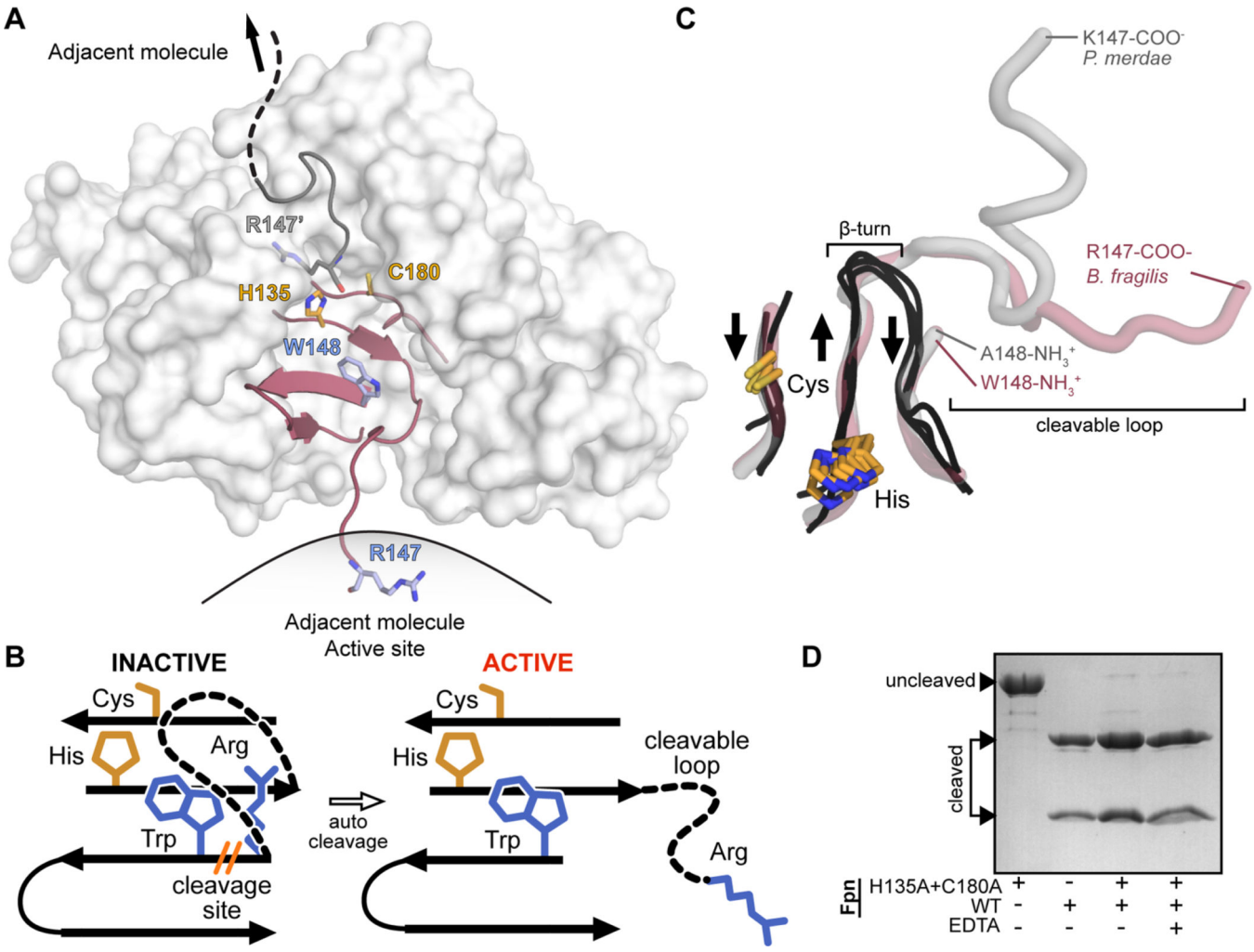

Figure 1.

B. fragilis Fpn active site and cleavable activation loop. Residue numbering includes the 19-amino acid predicted signal peptide present at the N-terminus of Fpn. (A) Surface representation of Fpn (white) with the β-strands constituting the active site colored maroon (PDB entry 5DYN). *B. fragilis* Fpn was crystallized in a cleaved form (cleavage site R147/W148, side chains colored light blue, catalytic dyad H135 and C180, side chains colored orange), with the cleaved region trapped in the active site of the neighboring molecule. (B) Cartoon representation of the *B. fragilis* Fpn active site and cleavable loop. When Fpn is inactive, the cleavable loop is intact and inhibits the active site composed of the catalytic dyad, H135 and C180 (orange sticks). Fpn is activated upon *cis* or *trans* loop cleavage between residues R147 and W148 (blue sticks), which modifies active site accessibility. (C) Superposition of the active site regions of legumain (PDB entry 4AW9), caspase-3 (PDB entry 1NMS), gingipain (PDB entry 4RBM), PmC11 (PDB entry 3UWS), and Fpn structures (PDB entry 5DYN). β-Strands composing the active sites of legumain, caspase-3, and gingipain are shown as black loops, and the equivalent regions in PmC11 and Fpn are show as transparent gray and red tubes, respectively. The aligned catalytic dyad side chains of cysteine and histidine are shown as orange sticks. The β-turn present in legumain,

caspase-3, and gingipain structures and the cleaved loops present at the equivalent position in PmC11 and Fpn structures are highlighted. Residues forming the termini of the cleavage sites are annotated. (D) Wild-type Fpn *trans* cleavage assay, in which Fpn was incubated with the active site mutant $Fpn^{H135A+C180A}$, in the presence (+) or absence (−) of EDTA.

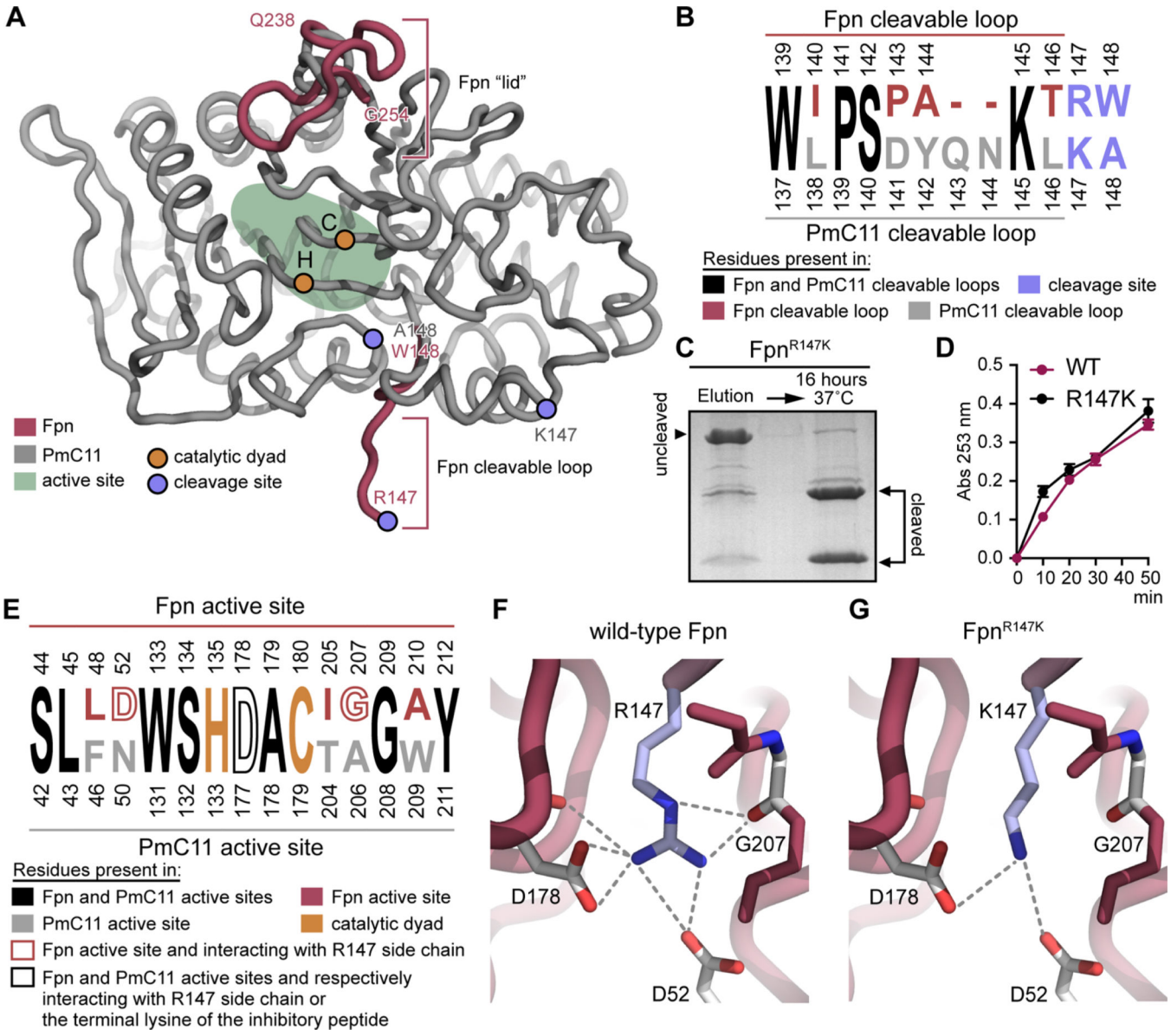

Figure 2.

Comparison of *B. fragilis* Fpn and *P. merdae* PmC11 structures. Residue numbering includes the 19-amino acid predicted signal peptide present at the N-terminus of Fpn. (A) Structural alignment of *P. merdae* PmC11 (PDB entry 3UWS) (gray) and *B. fragilis* Fpn (PDB entry 5DYN) (maroon). Only regions of Fpn that are structurally distinct from PmC11 are presented. Positions of catalytic dyad residues are colored orange; positions of cleavage site residues are colored blue, and the active site is delimited in light green. (B) Alignment of the amino acid residues present in *P. merdae* PmC11 and *B. fragilis* Fpn cleavable loops. Numbered residues are colored black when they are present in both PmC11 and Fpn, maroon when they are present in only Fpn, and gray when they are present in only PmC11. Basic residues present at the PmC11 and Fpn cleavage sites are colored light blue. (C) Autocleavage of Fpn^{R147K} immediately after purification and 16 h after purification at 37 °C. (D) BAEE cleavage assay. Cleavage of 1250 μM BAEE by 200 nM wild-type Fpn or

Fpn^{R147K} at 37 °C monitored at 253 nm. The experiment was conducted in triplicate; error bars represent standard deviations (mean ± standard deviation). (E) Alignment of residues present in *P. merdae* PmC11 and *B. fragilis* Fpn active sites. Numbered residues are colored black when they are present in both PmC11 and Fpn active sites, maroon when they are present in only the Fpn active site, and gray when they are present in only the PmC11 active site. Residues constituting the catalytic dyad are colored orange, and residues interacting with the arginine side chain in the Fpn structure (PDB entry 5DYN) and with the lysine side chain of the inhibitory peptide in the PmC11 structure (PDB entry 4YEC) are shown in empty maroon and black letters, respectively. (F) Polar interactions between the R147 side chain (blue stick) and the residues present in the Fpn active site (white sticks). (G) Model of the lysine side chain (blue stick) at position 147 in the Fpn active site and prediction of the polar interactions. Polar interactions were determined using PyMOL with a distance cutoff of 3.6 Å.

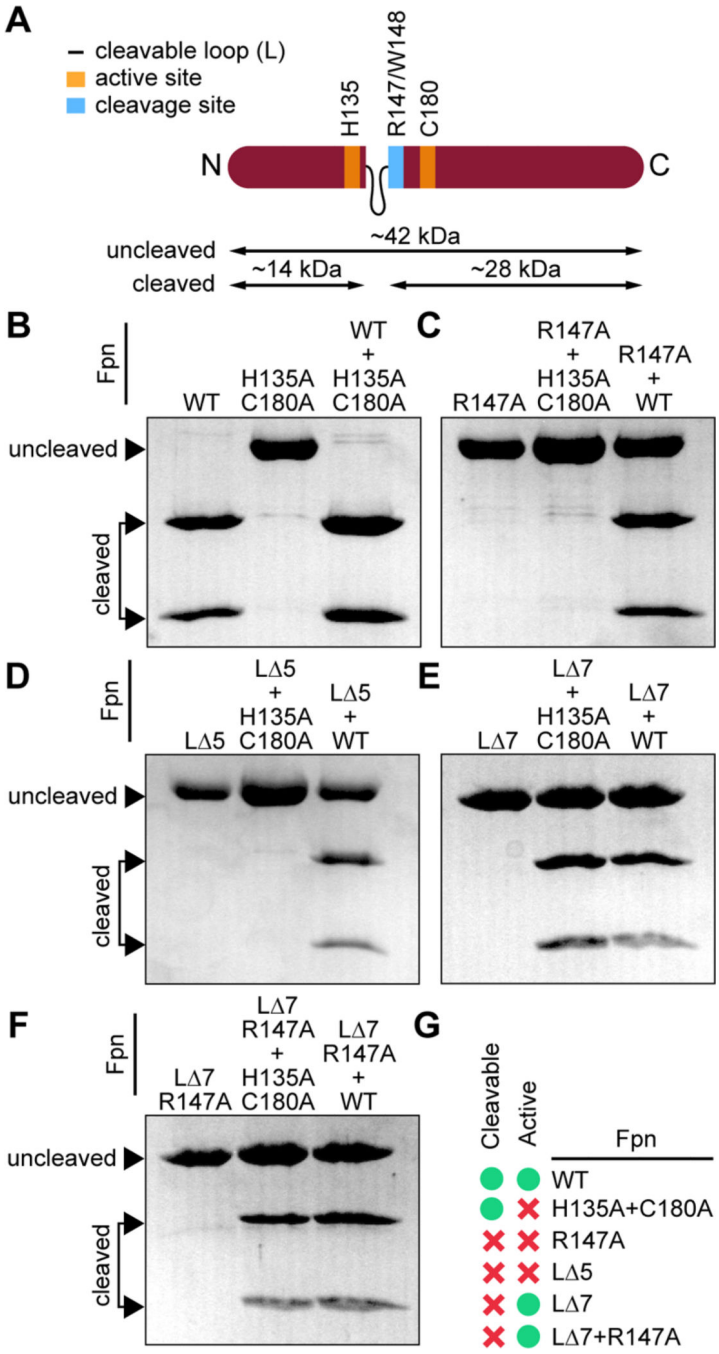

Figure 3.

Protease activity of Fpn active site and cleavage loop mutants. (A) Cartoon representation of the Fpn protein with the catalytic site (H135+C180) colored orange, the cleavage site (R147/W148) colored blue, and the cleavable loop represented as a thin black line. Sizes of the uncleaved protein (42 kDa) and of the two cleavage products (14 and 28 kDa) are delimited. The N- and C-termini are annotated. (B–F) Resolution of cleaved and uncleaved products by 14% SDS–PAGE. (B) Left lane, wild-type Fpn; middle lane, $Fpn^{H135A+C180A}$ (active site mutant); right lane, $Fpn^{H135A+C180A}$ cleaved by wild-type Fpn. (C) Left lane, Fpn^{R147A}

(cleavage site mutant); middle lane, $Fpn^{H135A+C180A}$ in the presence of inactive Fpn^{R147A}; right lane, Fpn^{R147A} in the presence of cleaved wild-type Fpn. (D) Left lane, $Fpn^{L\Delta5}$ (short deletion of the cleavable loop); middle lane, $Fpn^{H135A+C180A}$ in the presence of $Fpn^{L\Delta5}$; right lane, $Fpn^{L\Delta5}$ in the presence of cleaved wild-type Fpn. (E) Left lane, $Fpn^{L\Delta7}$ (full deletion of the cleavable loop); middle lane, $Fpn^{H135A+C180A}$ in the presence of $Fpn^{L\Delta7}$; right lane, $Fpn^{L\Delta7}$ in the presence of cleaved wild-type Fpn. (F) Left lane, $Fpn^{L\Delta7+R147A}$ (full deletion of the cleavable loop and cleavage site mutant); middle lane, $Fpn^{H135A+C180A}$ in the presence of active $Fpn^{L\Delta7+R147A}$; right lane, $Fpn^{L\Delta7+R147A}$ in the presence of cleaved wild-type Fpn. (G) Tabulation of Fpn active site and loop mutant peptidase activity and cleavability (green dot for activity and/or cleavability observed, red cross for no activity and/or cleavability observed).

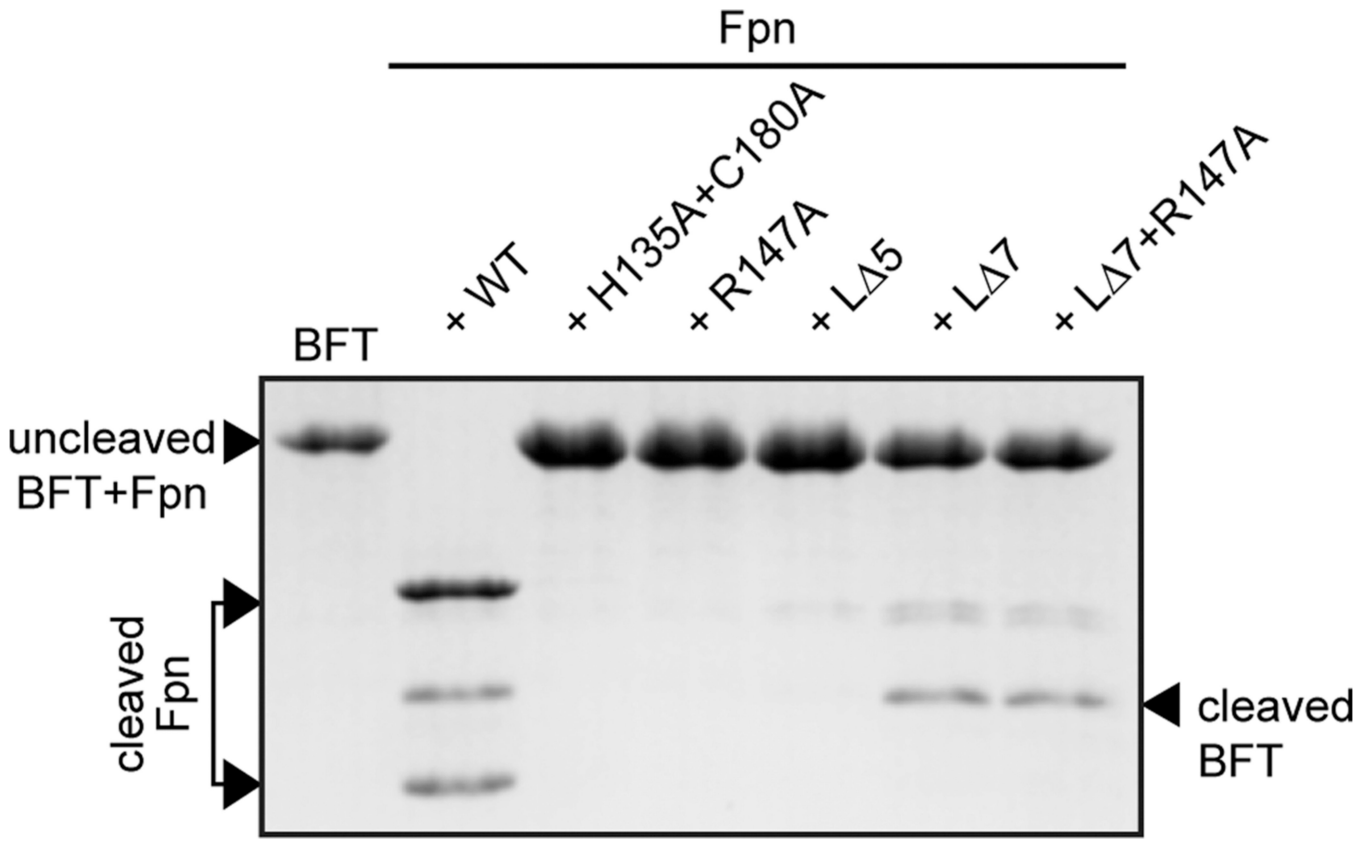

Figure 4.

Testing Fpn active site and loop mutants as proteases of the *B. fragilis* toxin, BFT. Wild-type Fpn cleavage of BFT results in a 17 kDa band on a SDS–PAGE gel. The active site mutant ($Fpn^{H135A+C180A}$), the cleavage site mutant (Fpn^{R147A}), and the loop mutant ($Fpn^{L\Delta5}$) do not process BFT after incubation at 37 °C for 45 min. A loopless mutant of Fpn ($Fpn^{L\Delta7}$) and a loopless mutant of Fpn harboring a substitution of the arginine residue at the loop cleavage site ($Fpn^{L\Delta7+R147A}$) cleave BFT.

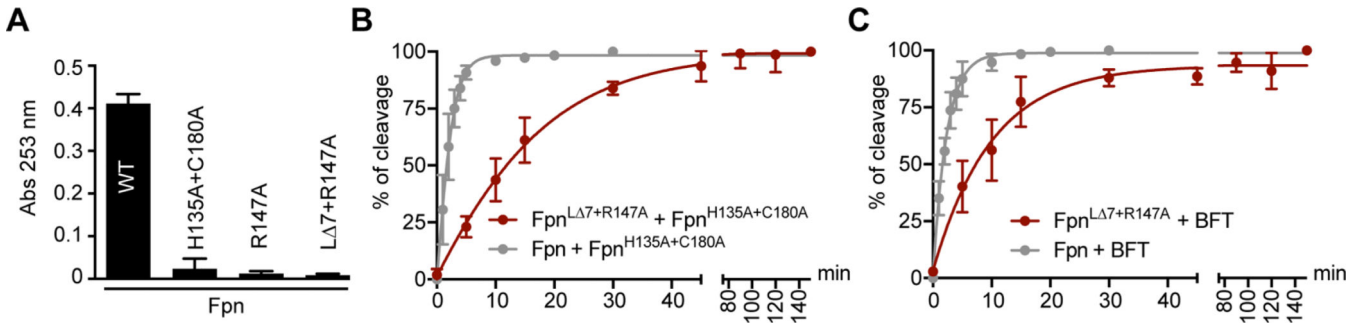

Figure 5.

Enzymatic activities of wild-type and mutant Fpn. (A) Absorbance at 253 nm representing the cleavage activities of 200 nM wild-type Fpn, $Fpn^{H135A+C180A}$, Fpn^{R147A}, or $Fpn^{L\Delta7+R147A}$ mutant proteins in the presence of 1250 μM synthetic substrate BAEE after incubation at 37 °C for 45 min. (B) Cleavage rate of purified $Fpn^{H135A+C180A}$ used as a substrate in the presence of wild-type Fpn (gray) or $Fpn^{L\Delta7+R147A}$ (maroon). (C) Cleavage rate of purified BFT used as a substrate in the presence of wild-type Fpn (gray) or $Fpn^{L\Delta7+R147A}$ (maroon). In panels A and B, each cleavage experiment was performed three times; error bars represent standard deviations (SD) (mean ± SD).